iScience

CellPress

Article

Infection Dynamics of a Bloom-Forming Alga and Its Virus Determine Airborne Coccolith Emission from Seawater

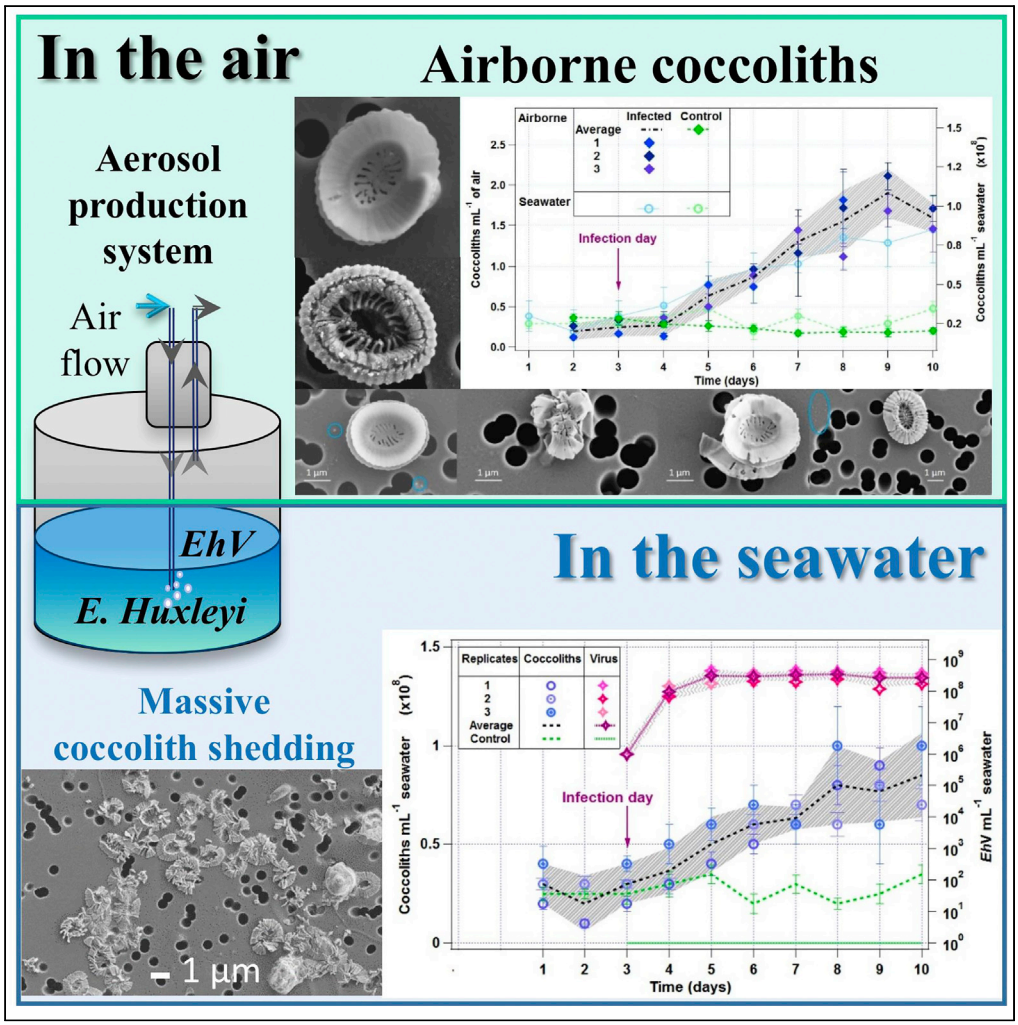

Miri Trainic, Ilan Koren, Shlomit Sharoni, Miguel Frada, Lior Segev, Yinon Rudich, Assaf Vardi

ilan.koren@weizmann.ac.il (I.K.)
assaf.vardi@weizmann.ac.il (A.V.)

HIGHLIGHTS

Oceanic microbial interactions affect key atmospheric processes

E. huxleyi viral infection induces coccolith shedding and emission to the air

Airborne coccolith emission occurs regularly, but increases during viral infection

Airborne coccoliths may be key contributors to coarse mode SSA

Trainic et al., iScience ■■, 1–9
■■, 2018
https://doi.org/10.1016/j.isci.2018.07.017

iScience

CellPress

Article

Infection Dynamics of a Bloom-Forming Alga and Its Virus Determine Airborne Coccolith Emission from Seawater

Miri Trainic,[1] Ilan Koren,[1,4,*] Shlomit Sharoni,[1] Miguel Frada,[3] Lior Segev,[1] Yinon Rudich,[1] and Assaf Vardi[2,*]

SUMMARY

Sea spray aerosols (SSA), have a profound effect on the climate; however, the contribution of oceanic microbial activity to SSA is not fully established. We assessed aerosolization of the calcite units (coccoliths) that compose the exoskeleton of the cosmopolitan bloom-forming coccolithophore, *Emiliania huxleyi*. Airborne coccolith emission occurs in steady-state conditions and increases by an order of magnitude during *E. huxleyi* infection by *E. huxleyi* virus (EhV). Airborne to seawater coccolith ratio is $1{:}10^8$, providing estimation of airborne concentrations from seawater concentrations. The coccoliths' unique aerodynamic structure yields a characteristic settling velocity of $\sim$0.01 cm s^{-1}, $\sim$25 times slower than average sea salt particles, resulting in coccolith fraction enrichment in the air. The calculated enrichment was established experimentally, indicating that coccoliths may be key contributors to coarse mode SSA surface area, comparable with sea salt aerosols. This study suggests a coupling between key oceanic microbial interactions and fundamental atmospheric processes like SSA formation.

INTRODUCTION

Sea spray aerosol (SSA), formed by primary emission from the ocean through bubble bursting (Woodcock et al., 1953), is the main component by mass of marine aerosols. It is one of the largest contributors to global aerosol mass and plays a pivotal role in the Earth's climate system (Lewis and Schwartz, 2004; Gantt and Meskhidze, 2013; Quinn et al., 2015). Generally, SSA is composed of an inorganic fraction, dominated by sea salt, and an organic component emitted from the vast carbon pool in the oceans, which may be internally or externally mixed with the sea salt component (Ault et al., 2013). The aerosolized organic matter can be composed of whole or fragments of marine microorganisms such as viruses, bacteria, and phytoplankton; may be the product of biological activity; or may result from the large reservoir of dissolved organic carbon in surface seawater that is not directly linked to local biological activity (Patterson et al., 2016; Aller et al., 2005; Facchini et al., 2008; Vignati et al., 2010; Ovadnevaite et al., 2011; Gantt and Meskhidze, 2013; Prather et al., 2013; Quinn et al., 2015). Despite great efforts directed toward resolving the effect of oceanic microbial activity, particularly phytoplankton, on SSA formation, many open questions remain about its role in SSA production mechanisms, chemical composition, effect on cloud physics, and climate (O'Dowd and De Leeuw, 2007; Gantt and Meskhidze, 2013; Quinn et al., 2015; Sharoni et al., 2015). The ocean's microbial activity exhibits large spatial and temporal variability, some of which is concentrated in the sea surface microlayer, the top 1 mm of the ocean (Kuznetsova et al., 2004; Aller et al., 2005; Cunliffe et al., 2011). To date, most field and laboratory studies have shown that the ocean's chemical composition during high biological activity (HBA) due to phytoplankton blooms is significantly different from that during low biological activity (LBA) (Guasco et al., 2014), specifically in terms of the dissolved organic matter content (Moran et al., 2016). Since the emitted SSA properties depend on the microlayer properties, the biological activity in the ocean may have a substantial impact on the size distribution and chemical composition of the emitted aerosols (Wang et al., 2015; O'Dowd et al., 2004; Leck and Bigg, 2005; Yoon et al., 2007; Fuentes et al., 2010; Gantt and Meskhidze, 2013; Prather et al., 2013). Although most studies show a dependence of SSA composition on biological activity (O'Dowd et al., 2004; Leck and Bigg, 2005; Yoon et al., 2007; Fuentes et al., 2010; Gantt and Meskhidze, 2013; Prather et al., 2013; Wang et al., 2015), a few studies claim that there is no significant effect of local biological activity on SSA (Collins et al., 2016), but rather that SSA properties are determined by the organic carbon pool due to the overall biological activity in the oceans (Quinn et al., 2014). It is therefore clear that the bulk effect of the ocean's biological component on SSA is not yet resolved. The level of complexity rises higher yet when attempting to examine the effect of the interactions within the ocean's microbial component on SSA, as in the few studies

[1]Department of Earth and Planetary Sciences, Weizmann Institute of Science, 234 Herzl Street, Rehovot 7610001 Israel

[2]Department of Plant and Environmental Sciences, Weizmann Institute of Science, 234 Herzl Street, Rehovot 7610001, Israel

[3]The Interuniversity Institute for Marine Sciences in Eilat & Silberman Institute of Life Sciences, Hebrew University of Jerusalem, Jerusalem, Israel

[4]Lead Contact

*Correspondence: ilan.koren@weizmann.ac.il (I.K.), assaf.vardi@weizmann.ac.il (A.V.)

https://doi.org/10.1016/j.isci.2018.07.017

Please cite this article in press as: Trainic et al., Infection Dynamics of a Bloom-Forming Alga and Its Virus Determine Airborne Coccolith Emission from Seawater, iScience (2018), https://doi.org/10.1016/j.isci.2018.07.017

that investigated the impact of microbial interactions within phytoplankton blooms on marine aerosols (Prather et al., 2013; O'Dowd et al., 2015; Sharoni et al., 2015). These studies demonstrated that averaging bulk biological activity by only comparing HBA to LBA cannot account for the full response of SSA to the complexity of oceanic biological systems and is missing a better resolution of specific microbial activity and their derived impact.

In this study, we use as a model phytoplankton the coccolithophore *Emiliania huxleyi*, which is the most dominant bloom-forming species of coccolithophore in the oceans, covering areas in scales of thousands of square kilometers (Balch et al., 1991; Tyrrell and Merico, 2004). *E. huxleyi* cells are covered by a calcite exoskeleton, composed of 2- to 4-μm-long $CaCO_3$ disks named coccoliths, which account for approximately a third of the total marine $CaCO_3$ production (Tyrrell and Merico, 2004; Iglesias-Rodriguez et al., 2008). *E. huxleyi* also plays a pivotal role in the global sulfur biogeochemical cycle in the ocean, and is responsible for high dimethyl sulfide (DMS) emission, a climatically active volatile organic compound that can generate secondary aerosols through atmospheric photochemical oxidation (Balch et al., 1991; Simo, 2001; Tyrrell and Merico, 2004; Beaufort et al., 2011). A rapid demise of *E. huxleyi* blooms in the oceans is often linked to viral infection by *E. huxleyi* virus (*Eh*V), a lytic large double-stranded DNA coccolithovirus (Phycodnaviridae) with a typical icosahedral structure and a diameter of 160–180 nm that specifically infects *E. huxleyi* cells. *E. huxleyi* bloom dynamics was suggested to have three phases, consisting of low *E. huxleyi* abundance, followed by exponential growth, and terminated by *E. huxleyi* cell demise during *Eh*V rise (Bratbak et al., 1993; Jacquet et al., 2002; Wilson et al., 2002a, 2002b; Vardi et al., 2012; Lehahn et al., 2014a, 2014b). Bloom demise following *E. huxleyi* cell lysis can occur over thousands of kilometers, accelerating the carbon turnover and determining the fate of phytoplankton biomass (Bratbak et al., 1993; Ziveri et al., 2000; Jacquet et al., 2002; Wilson et al., 2002b; Vardi et al., 2012; Lehahn et al., 2014a, 2014b). Viral infection leads to bloom demise and results in *E. huxleyi* cell death and enhanced shedding of coccoliths into the seawater (Balch et al., 1993; Wilson et al., 2002a, 2002b; Frada et al., 2008). High coccolith concentrations lead to higher reflectivity of the sea surface, giving the bloom area a characteristic milky blue color observed in satellite imagery (Holligan et al., 1983; Balch et al., 1991; Beaufort and Heussner, 1999; Tyrrell et al., 1999).

The abundance, biogeochemical importance, and ecological significance of *E. huxleyi* make it an ideal model organism for investigating the interaction between oceanic biology and atmospheric aerosols. Our laboratory setup allows to thoroughly investigate this interaction, examining each stage of *E. huxleyi* culture growth and demise. We monitored the effect of viral infection while simultaneously following the properties of aerosol emission into the air. We examined the effect of the different stages of *E. huxleyi* growth and demise, during viral infection or senescence, on SSA size distribution, their density, and their residence time.

RESULTS AND DISCUSSION

E. huxleyi strain RCC 1216 was infected by *E. huxleyi* virus strain 201 (*Eh*V201), and coccolith shedding into the seawater and emission to the air were monitored as a function of *E. huxleyi* cell abundance and *Eh*V concentration in the seawater. Control, non-infected *E. huxleyi* cultures were also monitored to assess the impact of different phases of growth on coccolith concentrations.

Upon infection, the *E. huxleyi* cells lose their coccolith shells due to a collapse of the coccolithophore structure, as clearly seen by the abrupt decrease in the concentration of calcified *E. huxleyi* cells and calcified cell percentage out of total cells immediately after infection (Figures 1A and 1B). One day post infection the percentage of calcified cells decreases dramatically, from an average of ~91% calcified cells to ~66%, whereas the control population remains at ~91% (Figures 1B and S1). The dramatic decrease in calcified population occurs even before any decrease in total cell count is observed. In fact, total *E. huxleyi* cell count increases on the first day after infection day by ~30%, as in the control cultures. For the control cultures, no abrupt changes in calcified cell concentrations are observed, although culture senescence gradually decreases the fraction of calcified cells (Figures 1A and 1B).

Coccolith concentrations were obtained from seawater samples collected on 0.2-μm Anodisc filters and measured throughout the experiment by light microscopy analysis (see methodology). Coccoliths were present in the seawater during all phases of *E. huxleyi* culture growth and demise, as expected for calcified

Please cite this article in press as: Trainic et al., Infection Dynamics of a Bloom-Forming Alga and Its Virus Determine Airborne Coccolith Emission from Seawater, iScience (2018), https://doi.org/10.1016/j.isci.2018.07.017

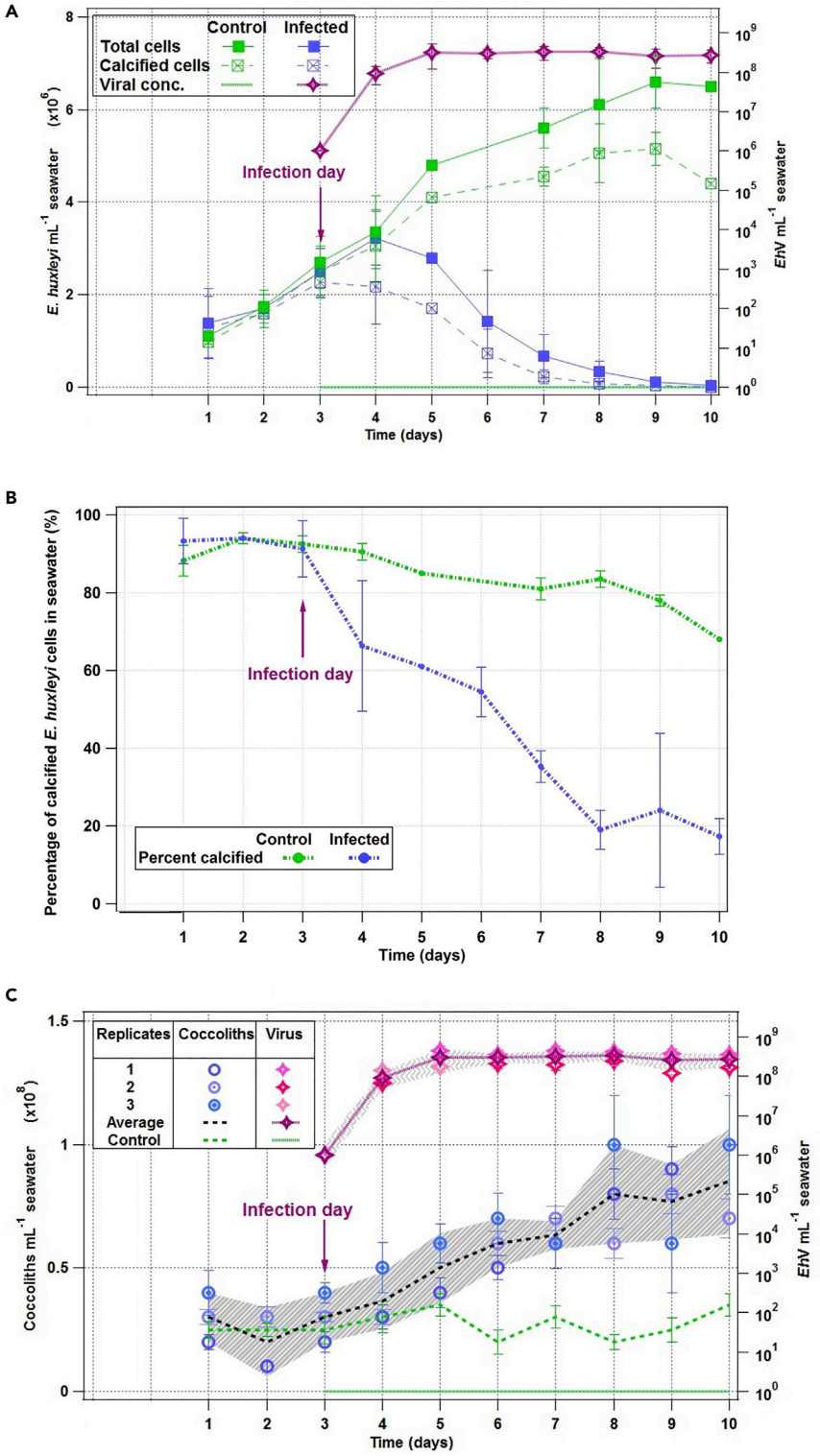

Figure 1. Dynamics of *E. huxleyi* and EhV, and Their Impact on Coccolith Release into Seawater

(A) *E. huxleyi* and EhV in seawater: total *E. huxleyi* cells and calcified cell concentrations (full and empty rectangles, respectively) for infected and control cultures over 10 days. The average viral concentrations are presented in log scale for reference. Error bars represent the standard deviation (SD) of three biological replicates.

Please cite this article in press as: Trainic et al., Infection Dynamics of a Bloom-Forming Alga and Its Virus Determine Airborne Coccolith Emission from Seawater, iScience (2018), https://doi.org/10.1016/j.isci.2018.07.017

Figure 1. *Continued*

(B) Percentage of calcified *E. huxleyi* cells in seawater: calcified cell percentage for infected and control populations. Error bars represent the SD of three biological replicates.

(C) Coccoliths and EhV in seawater: coccolith and viral concentrations for infected and control populations. Three biological replicates for infected population are presented: coccolith replicates are presented in circles, error bars represent the SD of technical replicates, viral replicates in diamonds, and the averages of the replicates are shown in dashed black and pink lines for coccoliths and viruses, respectively. The shaded areas around the averages represent the SD of the replicates. Note that viral concentrations are presented in log scale.

E. huxleyi strains, which are known to shed and regrow their coccolith-composed shells throughout their growth stages (Balch et al., 1993; Tyrrell and Merico, 2004).

For infected *E. huxleyi* cultures, coccolith concentration in the seawater increased gradually after viral infection (Figure 1C), following the dramatic decrease in the fraction of calcified cells (Figures 1A and 1B), as opposed to control cultures where coccolith concentration remained around $\sim 2 \times 10^7$ mL^{-1} (Figure 1C).

On the third day post the viral infection, the population diverged from the control culture and coccolith concentrations increased up to three-fold (Figure 1C).

To examine whether coccoliths are emitted into the air as SSA, and whether airborne coccoliths follow the trend observed in seawater, we used a bubbling system for SSA production (Sharoni et al., 2015) (see Figure 2). The coccolith flux from the bubbling system used in this study was validated by comparison with a different particle production system and was estimated to represent ambient conditions of particles flux in the North Atlantic (see Methods, and Transparent Methods, Figures S2 and S3, and Table S2). SSA were collected on 0.2-μm Anodisc filters and examined using polarized light microscopy (see Methods). Coccolith emission into the air was observed for both control and infected populations, and their concentrations and trends closely followed their seawater behavior (Figure 3). For virally infected populations, aerosolized coccolith concentrations reached up to ~2 coccolith particles mL^{-1} (particles cm^{-3}) of air, which is an order of magnitude higher than the control population. Coccolith concentration in seawater and air both reached maximal values on the fifth day post infection, when coccolith concentration was $>7 \times 10^7$ mL^{-1} in the seawater.

Aerosolized coccolith morphology throughout the experiment was examined by scanning electron microscopy, for infected and non-infected populations, using approximately 100 scanning electron microscopic images for analysis, containing ~500 coccoliths (see Figure 4). The average coccoliths' elliptic axes were 3.1 ± 0.6 μm for the major and 2.4 ± 0.6 μm for the minor axis, and therefore the eccentricity was 0.63 ± 0.05, consistent with previous studies (Young and Westbroek, 1991; Young and Ziveri, 2000; Young et al., 2014). Although viral infection triggered profound changes in coccolith concentration in seawater and air, no morphological changes in aerosolized coccoliths were observed between uninfected and infected cultures (Figure 4). The eccentricity remained the same throughout the experiment for both control and infected cultures. Using scanning electron microscopic analysis, we also measured the total area covered by aerosolized coccoliths on each filter compared with the total area covered by sea salt aerosol. We estimated the surface area, volume, and mass concentrations (mL^{-1}) of coccolith and sea salt particles captured in the scanning electron microscopic images (see Table 1).

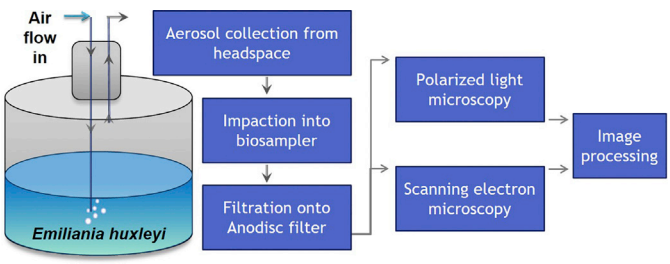

Figure 2. Schematic Presentation of the Experimental Setup Using the Bubbling System for Aerosol Production, Enumeration, and Morphological Measurement

Please cite this article in press as: Trainic et al., Infection Dynamics of a Bloom-Forming Alga and Its Virus Determine Airborne Coccolith Emission from Seawater, iScience (2018), https://doi.org/10.1016/j.isci.2018.07.017

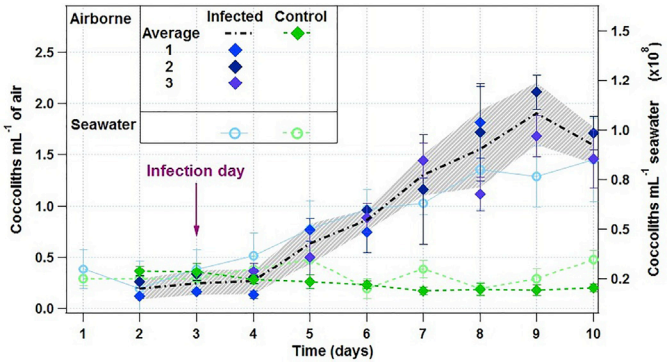

Figure 3. Dynamics of Airborne Coccolith Emission Compared with Detachment into Seawater

Coccolith airborne concentrations for infected and control populations over 10 days are presented. Three biological replicates for infected populations are shown (blue diamonds) the error bars represent the SD of technical replicates; the replicates' average is shown in dashed black line, and the shaded area around it represents their SD. Seawater coccolith average concentrations for control and infected cases are shown for comparison (circles). Control populations are presented in green, their error bars represent the SD of three biological replicates, and infected populations are shown in blue.

The overall surface area covered by airborne coccoliths before infection is similar to the area covered by sea salt aerosol; however, it is clearly dominated by coccolith particles post infection (Table 1). The total aerosolized coccolith surface area, volume, and mass concentrations increase by approximately one order of magnitude after infection with respect to non-infected cultures, in accordance with the increase in their number concentration (demonstrated in Figure 3). In both cases (Table 1 and Figure 3), the major increase in aerosolized coccolith is observed after 3 days post infection. These result were supported by data obtained from image analysis from both polarized light microscopy and scanning electron microscopy. Scanning electron microscopic image analysis also indicated that post infection, sea salt particle surface area, mass, and volume concentrations are higher than in the control, possibly due to changes in seawater chemical composition and surface tension (Blanchard, 1968; Cavalli et al., 2004; Sellegri et al., 2006; Fuentes et al., 2010; Collins et al., 2014; Quinn et al., 2015), which in our system may have been induced by viral infection (Suttle, 2005; Vardi et al., 2012). Airborne coccolith surface area and volume were substantially larger during viral infection (see Table 1) compared with sea salt particles. The implications of the higher surface area and volume concentrations of coccoliths compared with sea salt observed in these images may be significant for the importance of coccolith atmospheric emission compared with sea salt aerosol. Our results suggest that high-cell-density *E. huxleyi* blooms followed by demise due to viral infection may result in a coccolith contribution to atmospheric aerosol surface area larger than that of the sea salt. The coccolith contribution to surface area and volume concentrations of SSA may affect cloud microphysics and other climatic aspects.

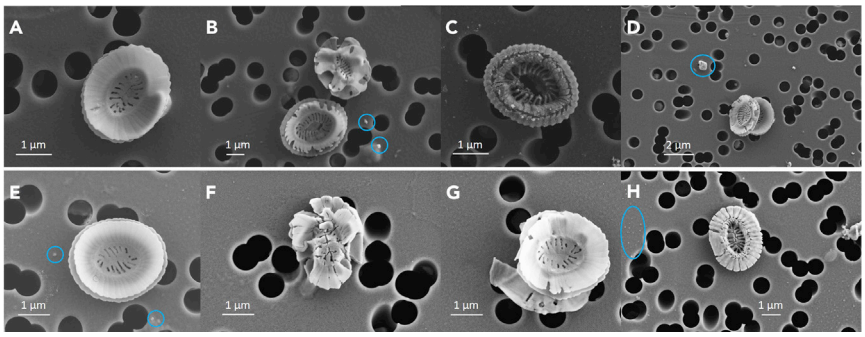

Figure 4. Scanning electron microscopic Images of SSA Collected on Polycarbonate Filters, Focusing on Aerosolized Coccolith Morphologies

Images of SSA emitted from non-infected (A–D), and virally infected (E–H) *E. huxleyi* cultures are presented. Coccolith morphologies appear whole or deformed for both infected and non-infected cultures. Sea salt aerosols are seen in the background (marked in blue circles).

Please cite this article in press as: Trainic et al., Infection Dynamics of a Bloom-Forming Alga and Its Virus Determine Airborne Coccolith Emission from Seawater, iScience (2018), https://doi.org/10.1016/j.isci.2018.07.017

	Days Post Infection	Coccolith Surface Area (μm^2 mL^{-1})[a]	Sea Salt Surface Area (μm^2 mL^{-1})[a]	Coccolith Volume (μm^3 mL^{-1})[b]	Sea Salt Volume (μm^3 mL^{-1})[c]	Coccolith Mass (pg mL^{-1})[d]	Sea Salt Mass (pg mL^{-1})[e]
	Control	2.9 ± 1.8	2.5 ± 1.4	2.1 ± 1.3	1.2 ± 0.7	0.6 ± 0.4	2.7 ± 1.6
Infected culture	2 days	2.2 ± 1.3	0.7 ± 0.8	1.5 ± 0.9	0.3 ± 0.4	0.5 ± 0.3	0.7 ± 0.9
	4 days	8.6 ± 6.9	2.5 ± 1.9	6.0 ± 4.8	1.3 ± 0.9	1.8 ± 1.4	2.7 ± 2.0
	5 days	15.0 ± 8.6	8.8 ± 2.8	10.5 ± 6.1	4.4 ± 1.4	3.2 ± 1.8	9.5 ± 3.1

Table 1. Surface Area, Volume, and Mass Concentrations for Airborne Coccolith and Sea Salt Particles Emitted from the Bubbling System, for Control and Infected Cultures

[a]Surface area was directly calculated using image analysis.

[b]Volume was calculated for coccoliths using estimation of thickness of 0.7 μm.

[c]For sea salt aerosols using an average diameter of 0.5 μm.

[d]Mass was calculated using a density of 0.3 pg/μm^3 for coccoliths (see Supplemental Information for calculation).

[e]Mass was calculated using a density of 2.17 pg/μm^3 for sea salt (Aylward and Findlay, 1999).

Atmospheric Implications of Coccolith Emission from Virally Infected Coccolithophores

Airborne coccoliths may affect marine atmospheric processes through their microphysical properties, their large size, and their unique morphology. It has also been observed that $CaCO_3$ from a biogenic source, such as in the case of coccoliths, contributes to aerosol and droplet alkalinity, which enhances atmospheric ozone reactions with sulfur dioxide in primary SSA and thereby reduces the role for DMS-derived (secondary) sulfur in nucleation (Sievering et al., 2004; Keene et al., 2007). Therefore, coccoliths may also alter chemical composition and induce such reactions when emitted as SSA. Moreover, $CaCO_3$ may react with gaseous HNO_3 to create $Ca(NO_3)_2$ particles, which can act as giant cloud condensation nuclei (GCCN) or as haze droplets, even at low relative humidity (Laskin et al., 2005).

The shape and morphology of coccoliths implies slow settling (terminal) velocity, which can significantly enhance their atmospheric residence time, hence increasing the likelihood for interactions with clouds (acting as CCN, GCCN, ice nuclei, or nuclei for haze droplets, as explained above) and for heterogeneous chemistry processes to take place on their surfaces. Per a given coccolith emission flux from the seawater to the atmosphere, residence times scale with overall concentrations. Therefore, longer residence times imply higher aerosol loading. The porous plate-like shape of the coccolith implies special aerodynamic properties. Non-spherical particles suspended in the atmosphere induce larger drag forces compared with spherical particles with similar volume (Yang et al., 2013). For suspended particles within the laminar flow regime (low Reynolds numbers) the drag forces can be scaled to the drag of equivalent sphere with a diameter of the longest dimension of the non-spherical particle (Cheng et al., 1988). In this dynamical regime, the terminal velocity (u) is proportional to the particle density and the square power of the particle radius (i.e., $u \sim \rho$, and $u \sim r^2$, where ρ and r are the particle density and radius, respectively) (Rogers and Yau, 1996). Replacing the coccolith shape with an equivalent sphere and preserving the coccolith mass yields an equivalent density that will be much smaller as most of the sphere will be empty. For an average coccolith with major axis of 3.1±0.6 μm, estimated volume of 4 μm^3 (4×10^{-6} cm^3), and density of 0.3 g cm^{-3} (see Table S1), we estimate that more than half of the equivalent sphere will be composed of air, reducing the equivalent sphere density to less than 0.15 g/cm^3, and therefore the fall velocity will be ~0.01 cm s^{-1}, which is in the terminal velocity range of much smaller spherical aerosols and is ~25 times slower compared with sea salt particles with the same dimension. Such differences in the settling velocities imply an enrichment of the coccolith fraction within the marine aerosol compared with sea salt. As a first approximation, the enrichment scales linearly with the ratio of the velocities. The real enrichment is likely to be much larger as the coccolith can reach higher atmospheric levels, and therefore reside longer in the atmosphere.

In this study, we examined the daily change in emission of aerosolized coccoliths from the water to the air as a function of *E. huxleyi*-virus interaction in the water. We demonstrate that during *E. huxleyi*

infection by *Ehv*, aerosol composition depends on the dynamics of host-virus interactions in the seawater (Figure 3). This is in agreement with recent studies, showing the changes of primary SSA properties due to changes in seawater microbial composition (Prather et al., 2013; O'Dowd et al., 2015; Sharoni et al., 2015). Our results show that aerosolized coccoliths emitted from *E. huxleyi* during viral infection may constitute a significant portion of the total SSA component, as coccolith surface area can exceed the surface area of pure sea salt aerosol (Figure 4, Table 1). Therefore, in terms of processes that depend on aerosol surface area (i.e., heterogeneous reactions, light scattering, cloud droplet formation), if emitted from a dense *E. huxleyi* population, coccoliths may be as important as sea salt aerosols.

In addition, we suggest a proxy to estimate coccolith aerosol number concentration in the ambient atmosphere. Coccoliths have been previously observed in the ambient marine atmosphere (Hawkins and Russell, 2010); however, no quantitative estimation of concentration has been provided. By using the ratio obtained from our model system of $\sim 1{:}10^8$ airborne to seawater coccoliths, we predict that under typical wind speeds in the North Atlantic, ambient coccolith concentration can reach ~ 1 coccolith mL^{-1} of air (10^3 L^{-1} air) during coastal oceanic blooms, when *E. huxleyi* cells reach seawater concentration of 10^4–10^5 cells mL^{-1} (Tyrrell and Merico, 2004), and therefore during demise may reach seawater coccolith concentrations of $\sim 10^7$–10^8 mL^{-1}. Coccolith emission into the air may be significant for several atmospheric processes, including those affecting atmospheric chemistry and cloud properties due to their morphology and their length (3.1 ± 0.6), which is larger than those of most coarse mode SSA (Sellegri et al., 2006; Prather et al., 2013; Quinn et al., 2015).

We note that bulk measurements of parameters such as Chlorophyll a (Chl-a), may be insufficient to determine the specific microbial activity in the oceans, which is highly dynamic in time and space. It is therefore of great importance to establish a model system for investigating the effect of microbial interactions (i.e., host-virus interactions) in phytoplankton population on aerosol emission and to resolve its impact by tracking microbial interactions in higher temporal resolution.

Ultimately, such approaches will enhance our understanding of the impact of these microscale biological interactions on large-scale ocean-atmosphere feedback processes.

METHODS

All methods can be found in the accompanying Transparent Methods supplemental file.

SUPPLEMENTAL INFORMATION

Supplemental Information includes Transparent Methods, three figures, and two tables and can be found with this article online at https://doi.org/10.1016/j.isci.2018.07.017.

ACKNOWLEDGMENTS

The authors acknowledge support by Scott Jordan and Gina Valdez, the De Botton Center for Marine Science, and the Minerva Foundation (Grant 712287).

AUTHOR CONTRIBUTIONS

I.K. and A.V. conceived the basic ideas and supervised the project; M.T. developed the concept and designed and performed the experiments; S.S., M.F., L.S., and Y.R. developed and performed additional laboratory, *in situ,* and model analyses; and M.T., Y.R., I.K., and A.V. wrote the paper.

DECLARATION OF INTERESTS

The authors declare no competing financial interests.

Received: April 6, 2018
Revised: June 19, 2018
Accepted: July 19, 2018
Published: August 15, 2018

REFERENCES

Aller, J.Y., Kuznetsova, M.R., Jahns, C.J., and Kemp, P.F. (2005). The sea surface microlayer as a source of viral and bacterial enrichment in marine aerosols. J. Aerosol. Sci. *36*, 801–812.

Ault, A.P., Moffet, R.C., Baltrusaitis, J., Collins, D.B., Ruppel, M.J., Cuadra-Rodriguez, L.A., Zhao, D.F., Guasco, T.L., Ebben, C.J., Geiger, F.M., et al. (2013). Size-dependent changes in sea spray aerosol composition and properties with different seawater conditions. Environ. Sci. Technol. *47*, 5603–5612.

Aylward, G., and Findlay, T. (1999). SI Chemical Data, Fourth Edition (John Wiley & Sons).

Balch, W.M., Holligan, P.M., Ackleson, S.G., and Voss, K.J. (1991). Biological and optical-properties of mesoscale coccolithophore blooms in the Gulf of Maine. Limnol. Oceanogr. *36*, 629–643.

Balch, W.M., Kilpatrick, K., Holligan, P.M., and Cucci, T. (1993). Coccolith production and detachment by *Emiliania huxleyi* (Prymnesiophyceae). J. Phycol. *29*, 566–575.

Beaufort, L., and Heussner, S. (1999). Coccolithophorids on the continental slope of the Bay of Biscay - production, transport and contribution to mass fluxes. Deep Sea Res. Part 2 Top. Stud. Oceanogr. *46*, 2147–2174.

Beaufort, L., Probert, I., de Garidel-Thoron, T., Bendif, E.M., Ruiz-Pino, D., Metzl, N., Goyet, C., Buchet, N., Coupel, P., Grelaud, M., et al. (2011). Sensitivity of coccolithophores to carbonate chemistry and ocean acidification. Nature *476*, 80–83.

Blanchard, C. (1968). Surface active organic material on airborne sea-salt particles. Bull. Am. Meteorol. Soc. *49*, 593.

Bratbak, G., Egge, J.K., and Heldal, M. (1993). Viral mortality of the marine alga *Emiliania huxleyi* (Haptophyceae) and termination of algal blooms. Mar. Ecol. Prog. Ser. *93*, 39–48.

Cavalli, F., Facchini, M.C., Decesari, S., Mircea, M., Emblico, L., Fuzzi, S., Ceburnis, D., Yoon, Y.J., O'Dowd, C.D., Putaud, J.P., et al. (2004). Advances in characterization of size-resolved organic matter in marine aerosol over the North Atlantic. J. Geophys. Res. Atmos. *109*, D24215.

Cheng, Y.S., Yeh, H.C., and Allen, M.D. (1988). Dynamic shape factor of a plate-like particle. Aerosol Sci. Technol. *8*, 109–123.

Collins, D.B., Bertram, T.H., Sultana, C.M., Lee, C., Axson, J.L., and Prather, K.A. (2016). Phytoplankton blooms weakly influence the cloud forming ability of sea spray aerosol. Geophys. Res. Lett. *43*, 9975–9983.

Collins, D.B., Zhao, D.F., Ruppel, M.J., Laskina, O., Grandquist, J.R., Modini, R.L., Stokes, M.D., Russell, L.M., Bertram, T.H., Grassian, V.H., et al. (2014). Direct aerosol chemical composition measurements to evaluate the physicochemical differences between controlled sea spray aerosol generation schemes. Atmos. Meas. Tech. *7*, 3667–3683.

Cunliffe, M., Upstill-Goddard, R.C., and Murrell, J.C. (2011). Microbiology of aquatic surface microlayers. FEMS Microbiol. Rev. *35*, 233–246.

Facchini, M.C., Rinaldi, M., Decesari, S., Carbone, C., Finessi, E., Mircea, M., Fuzzi, S., Ceburnis, D., Flanagan, R., Nilsson, E.D., et al. (2008). Primary submicron marine aerosol dominated by insoluble organic colloids and aggregates. Geophys. Res. Lett. *35*, L17814.

Frada, M., Probert, I., Allen, M.J., Wilson, W.H., and de Vargas, C. (2008). The "Cheshire Cat" escape strategy of the coccolithophore *Emiliania huxleyi* in response to viral infection. Proc. Natl. Acad. Sci. USA *105*, 15944–15949.

Fuentes, E., Coe, H., Green, D., de Leeuw, G., and McFiggans, G. (2010). On the impacts of phytoplankton-derived organic matter on the properties of the primary marine aerosol - part 1: source fluxes. Atmos. Chem. Phys. *10*, 9295–9317.

Gantt, B., and Meskhidze, N. (2013). The physical and chemical characteristics of marine primary organic aerosol: a review. Atmos. Chem. Phys. *13*, 3979–3996.

Guasco, T.L., Cuadra-Rodriguez, L.A., Pedler, B.E., Ault, A.P., Collins, D.B., Zhao, D.F., Kim, M.J., Ruppel, M.J., Wilson, S.C., Pomeroy, R.S., et al. (2014). Transition metal associations with primary biological particles in sea spray aerosol generated in a wave channel. Environ. Sci. Technol. *48*, 1324–1333.

Hawkins, L.N., and Russell, L.M. (2010). Polysaccharides, proteins, and phytoplankton fragments: four chemically distinct types of marine primary organic aerosol classified by single particle spectromicroscopy. Adv. Meteorol. *2010*, 612132.

Holligan, P.M., Viollier, M., Harbour, D.S., Camus, P., and Champagnephilippe, M. (1983). Satellite and ship studies of coccolithophore production along a continental-shelf edge. Nature *304*, 339–342.

Iglesias-Rodriguez, M.D., Halloran, P.R., Rickaby, R.E.M., Hall, I.R., Colmenero-Hidalgo, E., Gittins, J.R., Green, D.R.H., Tyrrell, T., Gibbs, S.J., von Dassow, P., et al. (2008). Phytoplankton calcification in a high-CO2 world. Science *320*, 336–340.

Jacquet, S., Heldal, M., Iglesias-Rodriguez, D., Larsen, A., Wilson, W., and Bratbak, G. (2002). Flow cytometric analysis of an *Emiliana huxleyi* bloom terminated by viral infection. Aquat. Microb. Ecol. *27*, 111–124.

Keene, W.C., Maring, H., Maben, J.R., Kieber, D.J., Pszenny, A.A.P., Dahl, E.E., Izaguirre, M.A., Davis, A.J., Long, M.S., Zhou, X., et al. (2007). Chemical and physical characteristics of nascent aerosols produced by bursting bubbles at a model air-sea interface. J. Geophys. Res. Atmos. *112*, D21202.

Kuznetsova, M., Lee, C., Aller, J., and Frew, N. (2004). Enrichment of amino acids in the sea surface microlayer at coastal and open ocean sites in the North Atlantic Ocean. Limnol. Oceanogr. *49*, 1605–1619.

Laskin, A., Iedema, M.J., Ichkovich, A., Graber, E.R., Taraniuk, I., and Rudich, Y. (2005). Direct observation of completely processed calcium carbonate dust particles. Faraday Discuss. *130*, 453–468.

Leck, C., and Bigg, E.K. (2005). Biogenic particles in the surface microlayer and overlaying atmosphere in the central Arctic Ocean during summer. Tellus B Chem. Phys. Meteorol. *57*, 305–316.

Lehahn, Y., Koren, I., Rudich, Y., Bidle, K.D., Trainic, M., Flores, J.M., Sharoni, S., and Vardi, A. (2014a). Decoupling atmospheric and oceanic factors affecting aerosol loading over a cluster of mesoscale North Atlantic eddies. Geophys. Res. Lett. *41*, 4075–4081.

Lehahn, Y., Koren, I., Schatz, D., Frada, M., Sheyn, U., Boss, E., Efrati, S., Rudich, Y., Trainic, M., Sharoni, S., et al. (2014b). Decoupling physical from biological processes to assess the impact of viruses on a mesoscale algal bloom. Curr. Biol. *24*, 2041–2046.

Lewis, E.R., and Schwartz, S.E. (2004). Sea Salt Aerosol Production: Mechanisms, Methods, Measurements and Models - a Critical Review (American Geophysical union).

Moran, M.A., Kujawinski, E.B., Stubbins, A., Fatland, R., Aluwihare, L.I., Buchan, A., Crump, B.C., Dorrestein, P.C., Dyhrman, S.T., Hess, N.J., et al. (2016). Deciphering ocean carbon in a changing world. Proc. Natl. Acad. Sci. USA *113*, 3143–3151.

O'Dowd, C., Ceburnis, D., Ovadnevaite, J., Bialek, J., Stengel, D.B., Zacharias, M., Nitschke, U., Connan, S., Rinaldi, M., Fuzzi, S., et al. (2015). Connecting marine productivity to sea-spray via nanoscale biological processes: phytoplankton dance or death disco? Sci. Rep. *5*, 14883.

O'Dowd, C.D., and De Leeuw, G. (2007). Marine aerosol production: a review of the current knowledge. Philos. Trans. A Math. Phys. Eng. Sci. *365*, 1753–1774.

O'Dowd, C.D., Facchini, M.C., Cavalli, F., Ceburnis, D., Mircea, M., Decesari, S., Fuzzi, S., Yoon, Y.J., and Putaud, J.P. (2004). Biogenically driven organic contribution to marine aerosol. Nature *431*, 676–680.

Ovadnevaite, J., O'Dowd, C., Dall'Osto, M., Ceburnis, D., Worsnop, D.R., and Berresheim, H. (2011). Detecting high contributions of primary organic matter to marine aerosol: a case study. Geophys. Res. Lett. *38*, L02807.

Patterson, J.P., Collins, D.B., Michaud, J.M., Axson, J.L., Sultana, C.M., Moser, T., Dommer, A.C., Conner, J., Grassian, V.H., Stokes, M.D., et al. (2016). Sea spray aerosol structure and composition using cryogenic transmission electron microscopy. ACS Cent. Sci. *2*, 40–47.

Prather, K.A., Bertram, T.H., Grassian, V.H., Deane, G.B., Stokes, M.D., DeMott, P.J., Aluwihare, L.I., Palenik, B.P., Azam, F., Seinfeld, J.H., et al. (2013). Bringing the ocean into the laboratory to probe the chemical complexity of sea spray aerosol. Proc. Natl. Acad. Sci. USA *110*, 7550–7555.

Quinn, P.K., Bates, T.S., Schulz, K.S., Coffman, D.J., Frossard, A.A., Russell, L.M., Keene, W.C., and Kieber, D.J. (2014). Contribution of sea surface carbon pool to organic matter enrichment in sea spray aerosol. Nat. Geosci. *7*, 228–232.

Quinn, P.K., Collins, D.B., Grassian, V.H., Prather, K.A., and Bates, T.S. (2015). Chemistry and related properties of freshly emitted sea spray aerosol. Chem. Rev. *115*, 4383–4399.

Rogers, R.R., and Yau, M.K. (1996). A short course in cloud physics, Third Edition (Elsevier Science Technology).

Sellegri, K., O'Dowd, C.D., Yoon, Y.J., Jennings, S.G., and de Leeuw, G. (2006). Surfactants and submicron sea spray generation. J. Geophys. Res. Atmos. *111*, D22215.

Sharoni, S., Trainic, M., Schatz, D., Lehahn, Y., Flores, M.J., Bidle, K.D., Ben-Dor, S., Rudich, Y., Koren, I., and Vardi, A. (2015). Infection of phytoplankton by aerosolized marine viruses. Proc. Natl. Acad. Sci. USA *112*, 6643–6647.

Sievering, H., Cainey, J., Harvey, M., McGregor, J., Nichol, S., and Quinn, P. (2004). Aerosol non-sea-salt sulfate in the remote marine boundary layer under clear-sky and normal cloudiness conditions: ocean-derived biogenic alkalinity enhances sea-salt sulfate production by ozone oxidation. J. Geophys. Res. Atmos. *109*.

Simo, R. (2001). Production of atmospheric sulfur by oceanic plankton: biogeochemical, ecological and evolutionary links. Trends Ecol. Evol. *16*, 287–294.

Suttle, C.A. (2005). Viruses in the sea. Nature *437*, 356–361.

Tyrrell, T., Holligan, P.M., and Mobley, C.D. (1999). Optical impacts of oceanic coccolithophore blooms. J. Geophys. Res. Oceans *104*, 3223–3241.

Tyrrell, T., and Merico, A. (2004). *Emiliania huxleyi*: bloom observations and the conditions that induce them. In Coccolithophores, H.R. Thierstein and J.R. Young, eds. (Springer). https://doi.org/10.1007/978-3-662-06278-4_4.

Vardi, A., Haramaty, L., Van Mooy, B.A.S., Fredricks, H.F., Kimmance, S.A., Larsen, A., and Bidle, K.D. (2012). Host-virus dynamics and subcellular controls of cell fate in a natural coccolithophore population. Proc. Natl. Acad. Sci. USA *109*, 19327–19332.

Vignati, E., Facchini, M.C., Rinaldi, M., Scannell, C., Ceburnis, D., Sciare, J., Kanakidou, M., Myriokefalitakis, S., Dentener, F., and O'Dowd, C.D. (2010). Global scale emission and distribution of sea-spray aerosol: sea-salt and organic enrichment. Atmos. Environ. *44*, 670–677.

Wang, X.F., Sultana, C.M., Trueblood, J., Hill, T.C.J., Malfatti, F., Lee, C., Laskina, O., Moore, K.A., Beall, C.M., McCluskey, C.S., et al. (2015). Microbial control of sea spray aerosol composition: a tale of two blooms. ACS Cent. Sci. *1*, 124–131.

Wilson, W.H., Tarran, G., and Zubkov, M.V. (2002a). Virus dynamics in a coccolithophore-dominated bloom in the North Sea. Deep Sea Res. Part 2 Top. Stud. Oceanogr. *49*, 2951–2963.

Wilson, W.H., Tarran, G.A., Schroeder, D., Cox, M., Oke, J., and Malin, G. (2002b). Isolation of viruses responsible for the demise of an *Emiliania huxleyi* bloom in the English Channel. J. Mar. Biol. Assoc. UK *82*, 369–377.

Woodcock, A.H., Kientzler, C.F., Arons, A.B., and Blanchard, D.C. (1953). Giant condensation nuclei from bursting bubbles. Nature *172*, 1144.

Yang, W.D., Marshak, A., Kostinski, A.B., and Varnai, T. (2013). Shape-induced gravitational sorting of Saharan dust during transatlantic voyage: evidence from CALIOP lidar depolarization measurements. Geophys. Res. Lett. *40*, 3281–3286.

Yoon, Y.J., Ceburnis, D., Cavalli, F., Jourdan, O., Putaud, J.P., Facchini, M.C., Decesari, S., Fuzzi, S., Sellegri, K., Jennings, S.G., et al. (2007). Seasonal characteristics of the physicochemical properties of North Atlantic marine atmospheric aerosols. J. Geophys. Res. Atmos. *112*.

Young, J.R., Poulton, A.J., and Tyrrell, T. (2014). Morphology of *Emiliania huxleyi* coccoliths on the northwestern European shelf - is there an influence of carbonate chemistry? Biogeosciences *11*, 4771–4782.

Young, J.R., and Westbroek, P. (1991). Genotypic variation in the coccolithophorid species *Emiliania huxleyi*. Mar. Micropaleontol. *18*, 5–23.

Young, J.R., and Ziveri, P. (2000). Calculation of coccolith volume and its use in calibration of carbonate flux estimates. Deep Sea Res. Part 2 Top. Stud. Oceanogr. *47*, 1679–1700.

Ziveri, P., Broerse, A.T.C., van Hinte, J.E., Westbroek, P., and Honjo, S. (2000). The fate of coccoliths at 48 degrees N 21 degrees W, northeastern Atlantic. Deep Sea Res. Part 2 Top. Stud. Oceanogr. *47*, 1853–1875.

ISCI, Volume ■ ■

Supplemental Information

Infection Dynamics of a Bloom-Forming Alga and Its Virus Determine Airborne Coccolith Emission from Seawater

Miri Trainic, Ilan Koren, Shlomit Sharoni, Miguel Frada, Lior Segev, Yinon Rudich, and Assaf Vardi

Supplementary Information

Transparent Methods

Culture growth and infection

E. huxleyi virus susceptible strain, RCC 1216, was used in this study (National Center of Marine Algae and Microbiota, NCMA). Cultures were grown in filtered, sterilized seawater collected from Michmoret, Israel (32.24°N, 34.52°E), and enriched with f/2 medium (Guillard and Ryther 1962), in polycarbonate carboys at 18°C with a 16:8 hours light:dark cycle. Light was provided by cool-white LED lights at an intensity of 80µM photons m^{-2} s^{-1}. *E. huxleyi* virus (*Eh*V) 201, isolated by Schroeder and colleagues (Schroeder et al. 2002) was used to infect the *E. huxleyi* 1216 cultures, since they are highly susceptible to *Eh*V 201 strain. Viral stocks were prepared by infecting *E. huxleyi* cultures until lysis, and filtering out the cell debris from the infected cultures using 0.45 µm PVDF filters (Millipore), and kept in the dark at 4°C. Exponential phase *E. huxleyi* cultures were infected with *Eh*V at a Multiplicity of Infection (MOI) of 1 viral particle per cell. The cultures were further incubated for 7 days. Culture harvesting for cell and viral enumeration, and aerosol collection were performed every 24 hrs.

Aerosol production by bubbling system

Aerosol production was obtained using a bubbling system similar to the one described in detail and validated (Sharoni et al. 2015) (see Figure 4). 5L of sample were constantly bubbled at a rate of 5 L min^{-1}. The emitted aerosols were collected for 24 hours into an impinger (BioSampler, SKC) containing 20ml of filtered sterilized seawater, onto which particles are impinged at constant high velocities. After 24 hours, the 20ml of seawater containing the aerosol sample was collected into a sterile plastic vial for coccolith enumeration. For coccolith detection by SEM (scanning electron microscopy) the aerosols from the bubbling system were directed into a filter holder (ferrule nut 3/8", PFA), and collected onto 0.8 µm polycarbonate membranes (47 mm, Millipore Co.).

For validation of our bubbling system, it was compared with a plunging waterfall system similar to those previously described in the literature (Sellegri et al. 2006, Prather et al. 2013, Quinn et al. 2015) (see supplementary methods, and figure S2) . The particle flux from the plunging waterfall system was found to be equivalent to SSA flux emitted by an estimated wind speed of approximately 8 m sec^{-1} (supplementary methods, and figure S3, table S1), a typical wind speed in the Atlantic Ocean (Hanley et al. 2010, Lehahn et al. 2014). The two systems were compared

for the same seawater media and culture conditions. The concentrations of the aerosolized coccoliths from virally infected population for the bubbling system and the new plunging waterfall system were 3.3±2.8 coccoliths mL^{-1}, and 7.7±2.7 coccoliths mL^{-1}, respectively. For the control populations, the aerosolized coccolith concentrations were 0.5±0.3 coccoliths mL^{-1} for the bubbling system, and 0.8±0.4 coccoliths mL^{-1} for the plunging waterfall.

We conclude that our bubbling system's coccolith production is equivalent to the waterfall system that produces particles at a flux equivalent to an estimated wind speed of ~8 m sec^{-1}, which is well within the typical environmental and meteorological conditions prevailing in the Atlantic Ocean (for more details see supplementary methods and figures S2, S3, table S1).

Enumeration in the seawater

Enumeration of *E. huxleyi* cells and viruses was performed with an Eclipse (iCyt) flow cytometer, with 488 nm excitation laser and 525 nm emission. *E. huxleyi* calcified and naked cells were analyzed using their chlorophyll fluorescence and side-scatter signatures (Figure S1). For *Eh*V detection, flow cytometric quantification of LVLP's (Large Virus Like Particles) was performed according to (Marie et al. 1999). This method was highly calibrated for enumeration specifically of *Eh*V.

Coccolith detection and enumeration

Coccolith detection and enumeration was performed with polarized light microscopy. Seawater samples both taken directly from the culture as well as the collected aerosol samples were filtered through a 25 mm Anodisc filter, pore size 0.2 µm (Whatman plc) using vacuum filtration, and left to dry completely. After drying, the filters were placed upon microscope slides, embedded with immersion oil and covered by a cover slip. The samples were examined with a cross-polarized light microscope (Nikon Polarizing Microscope Eclipse E600 POL) using a 60x oil immersion objective lens. The images were recorded, and coccolith enumeration was performed using image analysis software (Vision Builder for automated inspection, version 2013, National Instruments). SEM images for coccolith morphology were obtained by a Zeiss, FEG HR scanning electron microscope. 0.8 µm polycarbonate membranes containing the collected aerosol samples were mounted on an aluminum stub, sputter coated with Au–Pd as preparation prior to imaging.

Image analysis

Coccolith enumeration and determination of coccolith concentration from polarizer images, 5-20 images were obtained for each filter. Coccolith to sea salt aerosol ratios obtained from SEM

images were measured using the image analysis software (Vision Builder for automated inspection, version 2013, National Instruments), using approximately 100 SEM images to obtain the information. Coccolith and sea salt surface area were calculated from the data obtained by image analysis, and coccolith and sea salt aerosol volume and mass were evaluated.

Supplementary methods:

Calculation of single coccolith density and volume

Table S1. Coccolith and sea salt dimensions (volume, density and mass) (Related to Table 1). Coccolith dimensions were calculated using basic units (length, width, thickness, calcite density) taken from the literature. Coccolith volume and mass from (Young and Westbroek 1991, Young et al. 2014) are also presented for comparison. The coccolith dimensions are compared with sea salt.

Coccolith	**Feature value**	**units**	**Literature values**
length (diameter)	3.5	µm	
width (diameter)	3.1	µm	
thickness (diameter)	0.7	µm	
$CaCO_3$ density	2.7	pg/µm^3	
$CaCO_3$ volume	0.4*	µm^3	0.9-1.7 µm^3 **
$CaCO_3$ mass	1.2*	pg	2.3-4.6 pg **
ellipsoid volume	4.0	µm^3	
ellipsoid equivalent mass	10.7	pg	
coccolith density	0.30	pg/µm^3	
Sea salt (NaCl)	**Feature value**	**units**	
diameter (of cube)	1	µm	
NaCl volume	1	µm^3	
Nacl Density	2.17	pg/µm^3	
NaCl mass	2.17	pg	

* Calculated from a composition of single coccolith subunits

** Values obtained directly from (Young and Westbroek 1991, Young et al. 2014).

Calculation of coccolith and sea salt surface area, volume and mass concentrations for airborne particles emitted from the bubbling system:

Image analysis provided coccolith length, width, and number for each image. Image analysis also provided total area covered by coccoliths and by sea salt. That enabled the calculation of surface area, volume and mass concentrations. An example of the full calculation is provided in the supplemental dataset (SI coccolith conc calc.xlsx).

Validation of the coccolith concentration emitted by the bubbling system:

Our bubbling system was validated by comparison with a newly built plunging waterfall (weir) system that provides a size distribution typical of marine aerosol (Sellegri et al. 2006, Prather et al. 2013, Quinn et al. 2015). Supplementary figure S2 shows the size distribution of aerosol emitted from our plunging waterfall system using FSW (filtered sea water) compared to the size distributions published in (Sellegri et al. 2006, Prather et al. 2013) . The comparison shows that the size distribution produce by the plunging waterfall system is in accordance with the SSA production systems accepted in the field.

The particle flux from the plunging waterfall system is 6.8×10^5 m^{-2} sec^{-1} (see detailed calculation of the flux in table S2), which is equivalent to a wind speed of approximately 8 m sec^{-1} as seen in figure S3 (Fuentes et al. 2010); a typical wind speed in the Atlantic Ocean (Hanley et al. 2010, Lehahn et al. 2014). We point out that the wind speed estimation can only be treated as an approximation due to the limitations in its calculation; the particle flux was estimated using the plunging waterfall physical features, and the particle concentrations measured by the SMPS-APS online system, covering a wide particle size range of ~10 nm -20 µm. This flux calculation does not take into consideration particle losses in waterfall system walls. Additionally, the wind speed is equivalent to an estimated value based on figure 15 in (Fuentes et al. 2010). As can be seen in figure S3 adapted from figure 15, the fluxes are equivalent to a range of wind speeds, and vary substantially between different studies presented in the figure. Therefore, we treat the wind speed value we obtained (8 m sec^{-1}) as an estimation based on the calculations and assumptions elaborated here.

We compared the aerosolized coccolith concentration emitted by our bubbling system to the concentration emitted from the plunging waterfall for the same seawater/ culture conditions, by using the same collection and measurement method described in this paper for coccolith

enumeration using SEM image analysis (see materials and methods). The concentrations of the aerosolized coccoliths for the bubbling system used in this paper and the new plunging waterfall system we built are in the same order. Specifically, for virally infected populations the average aerosolized coccolith concentration obtained by SEM image analysis was 3.3±2.8 coccoliths mL^{-1} for the bubbling system, and 7.7±2.7 coccoliths mL^{-1} for the plunging waterfall. For the control populations the average aerosolized coccolith concentration obtained by SEM image analysis was 0.5±0.3 coccoliths mL^{-1} for the bubbling system, and 0.8±0.4 coccoliths mL^{-1} for the plunging waterfall.

We conclude that our bubbling system's coccolith production is equivalent to the waterfall system that produces particles at a flux equivalent to a wind speed of ~8 m sec^{-1}, which is well within the typical environmental and meteorological conditions prevailing in the Atlantic Ocean.

Supplementary figures:

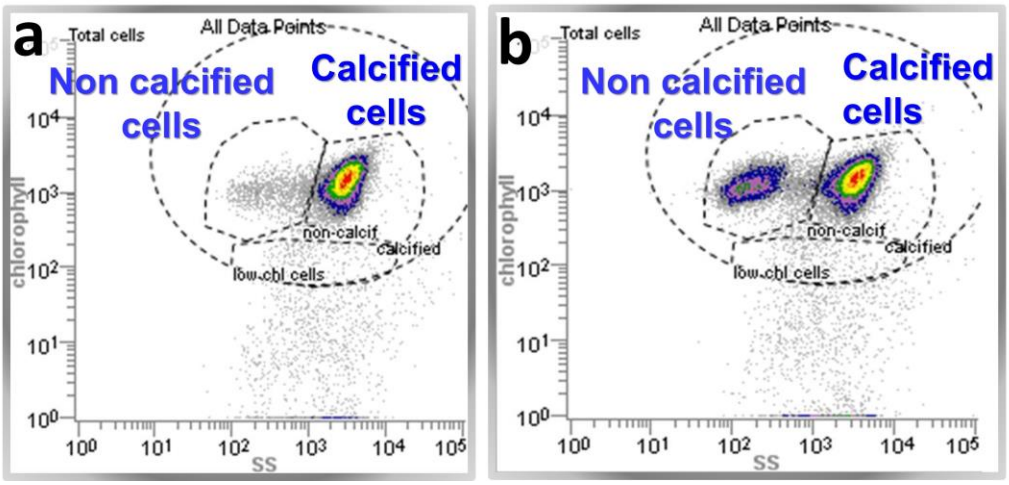

Figure S1: Flow cytometry data of Calcified and uncalcified fractions of E. huxleyi population *(Related to Figure 1). An example of flow cytometry analysis for calcified E. huxleyi population prior to infection is presented in (a), and one day after infection shown in (b). Calcified cells population density plot is shown on the right hand side of each panel and non-calcified are shown on the left. The average percentage of calcified cells during exponential growth for the three biological replicates presented in this study is 91%, decreasing one day post infection to 61% on average (see fig 1). This figure shows one of the replicates, with a decrease from 96% calcified population to 75% calcified one day post viral infection.*

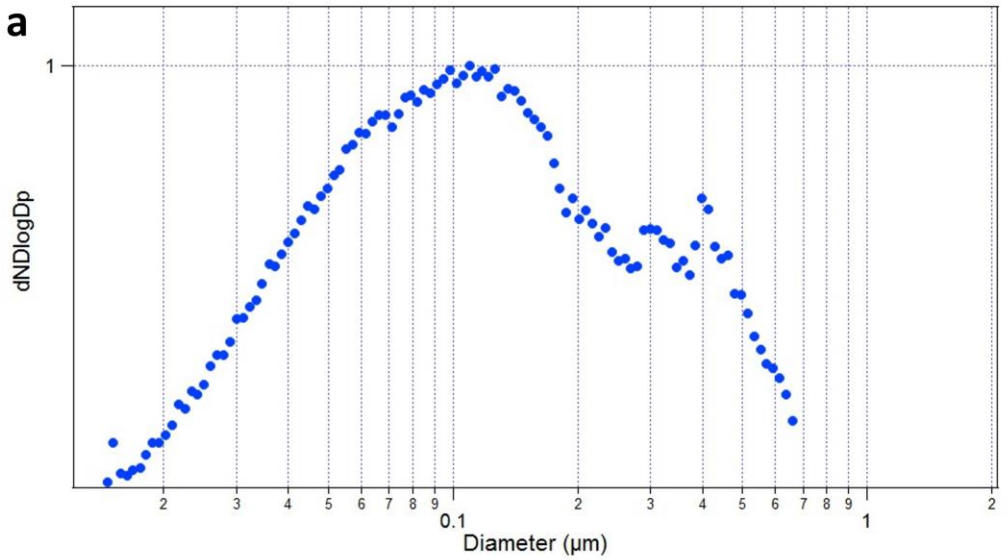
a
dNDlogDp
1
Diameter (μm)

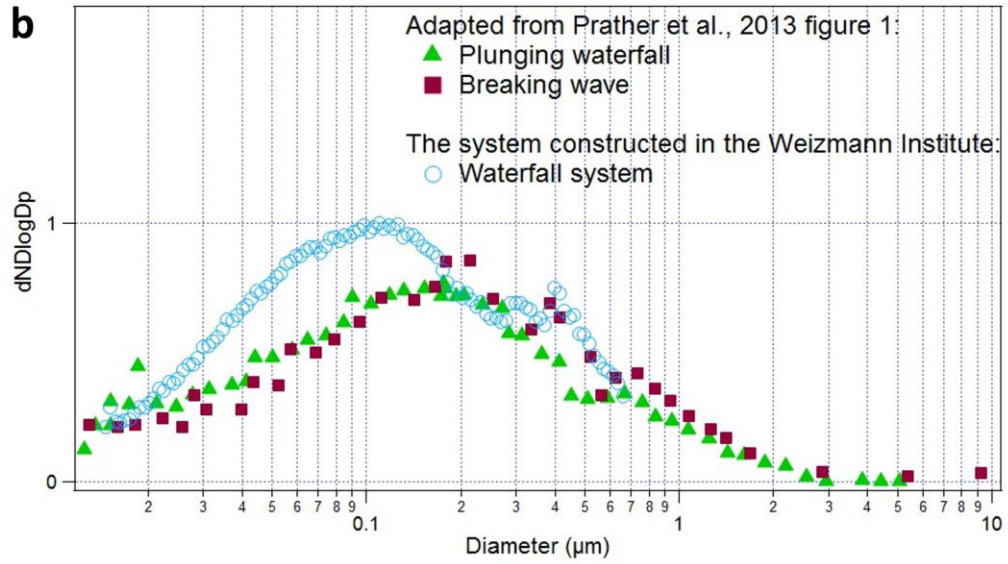
b
Adapted from Prather et al., 2013 figure 1:
Plunging waterfall
Breaking wave
The system constructed in the Weizmann Institute:
Waterfall system
dNDlogDp
Diameter (μm)

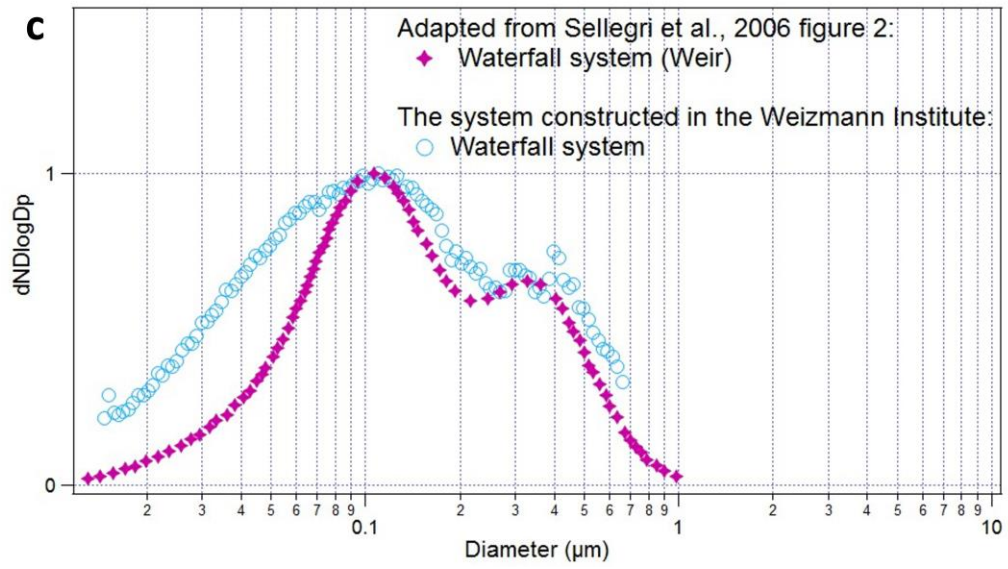
c
Adapted from Sellegri et al., 2006 figure 2:
Waterfall system (Weir)
The system constructed in the Weizmann Institute:
Waterfall system
dNDlogDp
Diameter (μm)

Figure S2: Size distributions emitted from various SSA production systems *(Related to Figure 4, Table 1). (a) The size distribution of SSA produced by the plunging waterfall system constructed at the Weizmann Institute. A comparison of the Weizmann waterfall size distribution (in light blue) with size distributions from other commonly used systems are presented: (b) Waterfall and breaking wave SSA production systems (Prather et al. 2013) (adapted from figure 1 of the paper), and (c) Weir SSA production system (Sellegri et al. 2006) (adapted from figure 2 in the paper).*

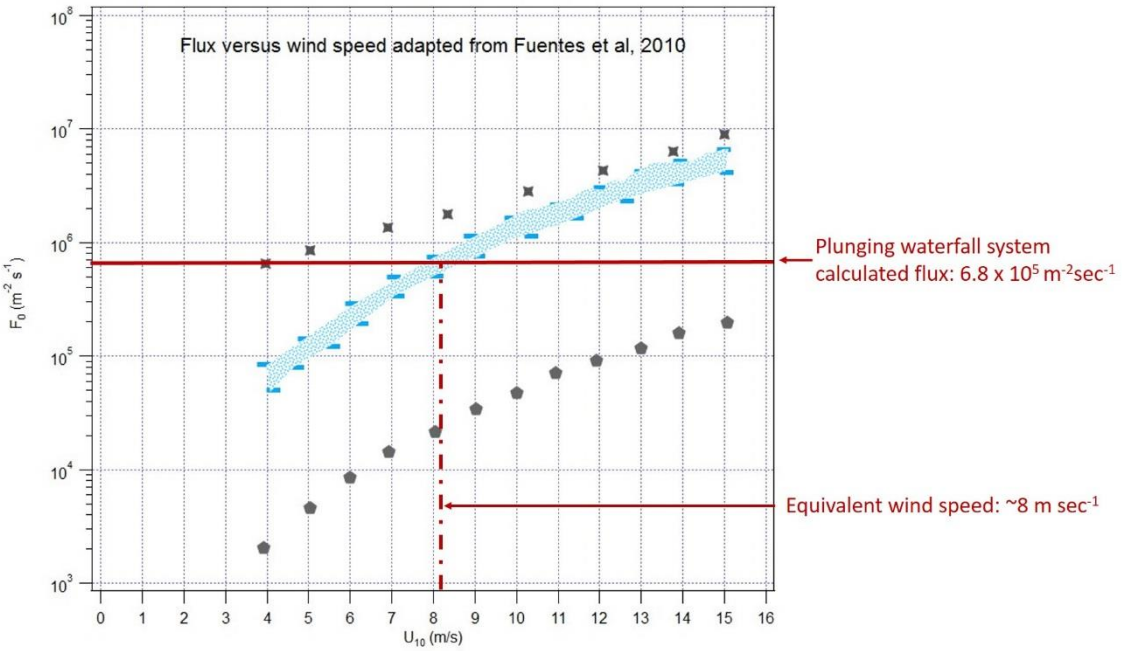

Figure S3: Particle flux versus wind speed *(Related to Figure 4, Table 1). The calculated particle flux produced by the plunging waterfall system equivalent to 6.8 x 10^5 m^{-2} sec^{-1} (marked by the solid red line) is superimposed on a graph adapted from figure 15 in Fuentes et al., 2010 (Fuentes et al. 2010), corresponds to a wind speed value of ~8 m sec^{-1}(dashed red line). The shaded light blue area represents the flux vs. wind speed results from the study conducted by Fuentes et al., 2010, while the grey stars and pentagons represent highest and lowest values, respectively, from other studies presented in figure 15 of the paper (Fuentes et al. 2010).*

Table S2: Plunging waterfall system flux calculation (Related to Figure 4, Table 1).

Waterfall system (carboy) dimensions:	value	equation
Total volume (Liters)	20	
Seawater volume (Liters)	6	
Headspace volume (Liters)	14	
Carboy radius (m)	0.125	
Seawater surface area (m^2)	0.049	πr^2
Air flowrate in the system (LPM)	1	
Air flowrate in the system (mL sec^{-1})	16.67	Fx1000/60
Total particle concentration (p mL^{-1}) *	2000	
Particle flowrate in the system (p sec^{-1})	3.3E+04	GxH
Particle flux in the system (p m^{-2} sec-1)	6.8E+05	I/E

* measured by SMPS and APS system, covering a size range of 10nm-20 micron particle diameter.

References:

Fuentes, E., H. Coe, D. Green, G. de Leeuw and G. McFiggans (2010). On the impacts of phytoplankton-derived organic matter on the properties of the primary marine aerosol - Part 1: Source fluxes. Atmospheric Chemistry and Physics **10**(19): 9295-9317.

Hanley, K. E., S. E. Belcher and P. P. Sullivan (2010). A Global Climatology of Wind-Wave Interaction. Journal of Physical Oceanography **40**(6): 1263-1282.

Lehahn, Y., I. Koren, Y. Rudich, K. D. Bidle, M. Trainic, J. M. Flores, S. Sharoni and A. Vardi (2014). Decoupling atmospheric and oceanic factors affecting aerosol loading over a cluster of mesoscale North Atlantic eddies. Geophysical Research Letters **41**(11): 4075-4081.

Prather, K. A., T. H. Bertram, V. H. Grassian, G. B. Deane, M. D. Stokes, P. J. DeMott, L. I. Aluwihare, B. P. Palenik, F. Azam, J. H. Seinfeld, et al. (2013). Bringing the ocean into the laboratory to probe the chemical complexity of sea spray aerosol. Proceedings of the National Academy of Sciences of the United States of America **110**(19): 7550-7555.

Quinn, P. K., D. B. Collins, V. H. Grassian, K. A. Prather and T. S. Bates (2015). Chemistry and Related Properties of Freshly Emitted Sea Spray Aerosol. Chemical Reviews **115**(10): 4383-4399.

Sellegri, K., C. D. O'Dowd, Y. J. Yoon, S. G. Jennings and G. de Leeuw (2006). Surfactants and submicron sea spray generation. Journal of Geophysical Research-Atmospheres **111**(D22).

Young, J. R., A. J. Poulton and T. Tyrrell (2014). Morphology of Emiliania huxleyi coccoliths on the northwestern European shelf - is there an influence of carbonate chemistry? Biogeosciences **11**(17): 4771-4782.

Young, J. R. and P. Westbroek (1991). GENOTYPIC VARIATION IN THE COCCOLITHOPHORID SPECIES EMILIANIA-HUXLEYI. Marine Micropaleontology **18**(1-2): 5-23.